Polymer Chemistry

ROYAL SOCIETY OF CHEMISTRY

PAPER

View Article Online
View Journal | View Issue

Cite this: *Polym. Chem.*, 2025, **16**, 3041

Poly(ε-L-lysine)-decorated particles with a tunable morphology by a combination of Ugi multicomponent polymerisation and RAFT-mediated PISA†

Thi Phuong Thu Nguyen, [a] Lei Lei, [a] Emily G. Dixon, [b] Clémence Le Coeur, [a,c] Vincenzo Taresco, [b] Antoine Debuigne [d] and Benoit Couturaud *[a]

Received 16th April 2025,
Accepted 26th May 2025

DOI: 10.1039/d5py00384a

rsc.li/polymers

We report herein the unprecedented combination of the Ugi multicomponent reaction (Ugi MCR) and Polymerisation-Induced Self-Assembly (PISA) to fabricate poly(ε-L-lysine) (PεLL) decorated amphiphilic nanoparticles. First, using the one-pot Ugi MCR of Boc-protected L-lysine with the addition of a trithiocarbonate (TTC) compound, a macromolecular chain transfer agent (macroCTA) for Reversible Addition–Fragmentation chain-Transfer (RAFT) polymerisation was synthesised. The obtained PεLL-TTC was then used for chain extension of the hydrophobic 2-hydroxypropyl methacrylate (HPMA) in water. The reaction proceeded *via* the PISA mechanism, leading to the formation of amphiphilic block copolymers that self-assembled into a variety of morphologies—including spheres, short worm-like structures, and vesicles—spanning sizes from below 100 nm to over 1 μm. This work showcases a proof-of-concept to prepare water-dispersed nanoparticles decorated with polypeptoids, which are highly desired in biological applications (*e.g.* stealth-cargo in nanomedicine, bio-separation, antibacterial coating, *etc.*).

Introduction

Polymerisation-Induced Self-Assembly (PISA) has emerged as a powerful technique for generating self-assembled nanoparticles, particularly in aqueous media, aligning with environmentally friendly practices. During PISA, the chain extension of a hydrophilic polymer block with hydrophobic monomers triggers *in situ* self-assembly, yielding nanostructures such as spherical micelles, fibers, worm-like particles, vesicles, and lamellas.[1] Unlike traditional methods requiring volatile organic solvents, PISA offers a sustainable alternative for biomedical applications.[2] For the purpose of chain-extension, PISA is dominantly coupled with controlled polymerisation techniques, including atom transfer radical polymerisation, nitroxide-mediated polymerisation, ring-opening metathesis polymerisation, and ring-opening polymerisation, but predominantly with Reversible-Addition Fragmentation chain Transfer (RAFT) polymerisation.[3–7] Typically, a hydrophilic macro-chain transfer agent (macroCTA) is synthesised in an organic solvent before initiating PISA.[8–11] While polyethylene glycol, poly(meth)acrylamides and poly(meth)acrylates are common macroCTAs, only a few examples of alternatives are described in the literature.[12]

Polypeptoids, due to their structural similarity to natural polypeptides, are promising candidates for PISA-based biomaterials, offering biocompatibility, stability, and tunable functionality.[13–15] Polypeptoids can be synthesised *via* solid-phase synthesis or through the ring-opening polymerisation of *N*-carboxyanhydrides.[16–18] These methods have been combined with PISA to produce water-soluble coronas or hydrophobic cores. However, while solid-phase synthesis is effective for short oligomers, it requires labor-intensive protection–deprotection steps, whereas ring-opening polymerisation demands complex monomer synthesis and stringent reaction conditions.[19] In contrast, the Ugi multicomponent reaction (Ugi MCR) provides an efficient route to obtain polypeptoids with atom economy, mild conditions, and broad structural diversity.[20–24] Extensively applied in various fields,[25–29] this approach has proven particularly useful for polymerisation of amino acids. For example, Zhang *et al.* synthesised γ-, δ-, and

[a]*Univ Paris Est Creteil, CNRS, Institut de Chimie et des Matériaux Paris-Est (ICMPE), UMR 7182, 2 rue Henri Dunant, 94320 Thiais, France. E-mail: benoit.couturaud@cnrs.fr*
[b]*School of Chemistry, University Park, Nottingham NG7 2RD, UK*
[c]*Laboratoire Léon Brillouin, CEA-CNRS (UMR-12), CEA Saclay, Université Paris-Saclay, 91191 Gif-sur-Yvette Cedex, France*
[d]*Center for Education and Research on Macromolecules (CERM), University of Liege (ULiege), Quartier Agora, 13 Allée du Six Août, Sart-Tilman, B-4000 Liège, Belgium*

† Electronic supplementary information (ESI) available. See DOI: https://doi.org/10.1039/d5py00384a

ε-polypeptoids from bifunctional amino acids for drug encapsulation,[30] while Debuigne's group developed alternating polypeptide–polypeptoid copolymers and explored their functionalisation.[31,32] Tao *et al.* further confirmed the polycondensation nature of the Ugi MCR, leading to the formation of alternating polypeptoids and polyampholytes.[33] Among diverse polypeptoids that can be obtained by the Ugi MCR, PεLL is of great interest for further investigation. Resulting from the biosynthesis of various microorganisms,[34,35] naturally existing PεLL is known for its antimicrobial activity, heat stability and low toxicity. The functionalisation of PεLL has, thus, attracted continued interest for various applications in the medical field.[36–38] For this purpose, along with other chemosynthetic routes for the functionalisation of PεLL,[30,39] the Ugi MCR has emerged as a promising technique for synthesising polymers while enabling the introduction of new functionalities.

The combination of the Ugi MCR with controlled radical polymerisation has been reported in the literature. For example, the group of Tao has described the use of the Ugi MCR to graft polymers on carbon nanotubes,[40] to conjugate polymers with proteins,[41] or to prepare miktoarm polymers[42] by RAFT polymerisation. Despite the efficiency of the Ugi MCR in polypeptoid synthesis, the use of the Ugi MCR to prepare hydrophilic blocks for PISA-RAFT remains unexplored.

In this work, we demonstrate the one-pot synthesis of a macroCTA trithiocarbonate (TTC) derived from PεLL using the Ugi MCR, hereinafter referred to as PεLL-TTC. The obtained PεLL-TTC is characterised by various techniques (NMR, SEC, UV-Vis, and MALDI-ToF) to confirm the chain-end fidelity and the molar mass. PεLL-TTC is then employed as a hydrophilic block for chain extension with the hydrophobic HPMA in water at 55 °C with systematic changes in mass content and degree of polymerisation (DP) of the PHPMA block. Formation of particles is observed during the polymerisation and characterised by various analyses including dynamic light scattering (DLS), transmission electron microscopy (TEM), and when adapted small angle X-ray scattering (SAXS).

Experimental

Materials

Unless otherwise stated, all chemicals are used as received. KOH (Sigma Aldrich), acetone (pure, Carlo Erba), ethanethiol (97% pure, Alfa Aesar), carbon disulfide (99.9%, Alfa Aesar), 4-toluenesulfonyl chloride (PTSC), dichloromethane (pure, stabilised with amylene, Carlo Erba), 4,4′-azobis(4-cyanovaleric acid) (AICV, 98% pure, Sigma Aldrich), *tert*-butyloxycarbonyl-L-lysine (Boc-Lys) (97% pure, Alfa Aesar), formaldehyde (37 wt% in water with 10–15% methanol as a stabiliser, Thermo Scientific), *tert*-butyl isocyanide (98% pure, Sigma Aldrich or 97%, Thermo Scientific), diethyl ether (pure, stabilised with BHT), trifluoroacetic acid (99% pure, Thermo Scientific), 2,2′-azobis(2-methylpropionamidine) dihydrochloride (V-50, granular, 99% pure, Aldrich), 2-hydroxypropyl methacrylate (HPMA, 98% pure, mixture of isomers, stabilised by 0.02% 4-methoxyphenol, Alfa Aesar), and methanol (anhydrous, Carlo Erba). HPMA was filtered over silica gel to remove the stabiliser before use.

Methods

Synthesis of 4-cyano-4-[[(ethylthio)thioxomethyl]thio]pentanoic acid (CEPA). CEPA was synthesised as reported in the literature.[43] In brief, KOH (6.72 g, 0.07 mol) was dissolved in 25 mL of an acetone : water (20 : 5 v/v) mixture in a round bottom flask. Ethanethiol (7.4 mL, 0.10 mol) was added to the mixture under stirring. The flask was then cooled down in an acetone bath followed by the addition of carbon disulfide (6 mL, 7.61 g, 0.10 mol). After 45 minutes of stirring, PTSC (9.91 g, 0.052 mol) was added to the mixture and then stirred at room temperature for 1 hour. The mixture was then heated to 45 °C and stirred for 30 minutes. The remaining was then diluted in 150 mL of dichloromethane and washed with 50 mL of distilled water (twice). The volatile compounds were eliminated by evaporation under a fume hood, and an orange crude product was obtained. AICV (15.2 g, 0.053 mol) was added to the crude product followed by the addition of 300 mL of ethyl acetate. The whole mixture was then degassed with argon, stirred and then heated to 75 °C with reflux for 20 hours. The mixture was cooled down to room temperature and the solvent was then evaporated using a stream of argon. The final product was obtained by column chromatography on silica gel using a gradient solvent mixture of cyclohexane and dichloromethane with >99% dichloromethane at the end. The purified product was obtained as an orange solid after evaporation of the solvent. ^{1}H-NMR: DMSO-d_6, 400 Hz, δ: 1.36 ppm (triplet, 3H, CH_3–CH_2–), 1.88 ppm (singlet, 3H, CH_3–C(CN)–), 2.40–2.53 ppm (m, 2H, –C(CN)–CH_2–), 2.69 ppm (m, –CH_2–COOH), 2.35 ppm (quartet, 2H, CH_3–CH_2–S–C(=S)–S).

Synthesis of Boc-PεLL-TTC. In a 10 mL round bottom flask, CEPA (0.10 g, 0.38 mmol, 0.05 eq.) was weighed followed by Boc-Lys (1.78 g, 7.21 mmol, 0.95 eq.); then 8 mL of methanol : H_2O (1 : 1 v/v) was added and the mixture was stirred using a magnetic bar. Formaldehyde (9.87 mmol, 1.3 eq.) was added to the mixture using a micropipette, resulting in full dissolution of all solids. Finally, with precaution, *tert*-butyl isocyanide (9.87 mmol, 1.3 eq.) was added dropwise to the reaction mixture using a micropipette. The flask was secured and closed with a septum. The reaction proceeded at room temperature. After 24 hours, phase separation was observed. The polymers (Boc-PεLL-TTC) were isolated by discarding the transparent aqueous phase. The crude polymer was then diluted in methanol prior to precipitation in cold diethyl ether. After filtration through a Büchner funnel under reduced pressure, a light-yellow powder was obtained and subsequently dried under vacuum to yield purified Boc-PεLL-TTC (yield: 30%).

Deprotection of Boc-PεLL-TTC to obtain PεLL-TTC. 400 mg of Boc-PεLL-TTC was charged into a 10 mL round bottom flask with a stirring bar. The polymer was dissolved in 1 mL of molecular-sieve-dried dichloromethane. The flask was then immersed in an ice bath. 1 mL of trifluoroacetic acid was added dropwise to the reaction mixture. After 3–4 hours, the

reaction mixture was concentrated by rotary evaporation. The PεLL-TTC polymer was retrieved by precipitation in cold diethylether and dried under vacuum to obtain a light yellow powder (yield: 90%).

PISA-RAFT chain extension of PεLL-TTC with HPMA. A typical PISA-RAFT chain extension of PεLL-TTC with HPMA was carried out as follows: for a target degree of polymerisation (DP_0) of 200 and polymerisation at 5 wt% of the monomer: 10 mg of PεLL-TTC ($M_{n,UV}$ = 2900 g mol^{-1}, 5 × 10^{-3} mmol) was weighed into a vial. Then 2.550 mL of Milli-Q water was added to dissolve the macroCTA followed by the addition of 0.250 mL of an aqueous solution containing 0.27 mg of V-50. Finally, 0.140 mL of HPMA was added into the reaction mixture. The vial was then closed with a silicon septum. The reaction mixture was stirred and degassed with a moderate flow of argon for 15 minutes. After degassing, the polymerisation commenced as soon as it was immersed in a preheated oil bath at 55 °C. The polymerisation was quenched by exposure to air after 21 hours of reaction, with >90% monomer conversion confirmed by ^{1}H NMR analysis.

Kinetics of PISA-RAFT chain extension of the PεLL macroCTA with HPMA. The kinetics of chain extension of the $PεLL_{2.9k}$ macroCTA with HPMA in water was studied at DP_0 = 100 with 5 wt% in a 5 mL vial. First, 10.8 mg of V-50 was dissolved in 10 mL of Milli-Q water as a stock solution. 0.5 mL of the initiator stock solution (0.54 mg of V-50, 2.0 × 10^{-6} mol, 0.2 eq.) was transferred into a vial containing 29 mg of $PεLL_{2.9k}$ (1.00 × 10^{-5} mol, 1.0 eq.) and a magnetic stirring bar. 2.30 mL of Milli-Q water was added to the vial followed by the addition of 0.140 mL of HPMA (0.144 g, 1.00 × 10^{-3} mol, 100 eq., 5 wt%). The vial was closed with a silicone septum and degassed with argon for 15 minutes at room temperature. Argon was removed at the end of degassing and the vial was sealed with parafilm and then immersed in a preheated oil bath at 55 °C to start the kinetics studies. An aliquot (200 μL) of the reaction mixture was taken at regular intervals using a degassed disposable syringe for NMR, SEC, and DLS analyses.

Characterisation

NMR spectroscopy. NMR was carried out using a Bruker 400 MHz spectrometer. The polymer concentration was 20 mg per 1 mL of deuterated solvent and the measurement was carried out in a 5 mm tube. The spectra were analysed using MestReNova 5.3.0 (Mestrelab Research S.L.). Chemical shifts are reported in *ppm*.

Size exclusion chromatography. The molar mass of the polymers was determined using size exclusion chromatography (SEC) in DMF (+NH_4BF_4 5 mM) as the eluent at 50 °C. SEC analyses were performed using a Shimadzu instrument fitted with a mixed-C column and an RI detector. The molar mass in number (M_n), molar mass in weight (M_w) and molar mass dispersity ($Đ$) were calculated using poly(ethylene glycol) (PEG) standards with the molecular weight in the range of 610 g mol^{-1} to 15 110 000 g mol^{-1}.

UV-Visible spectroscopy. Absorbance measurements of solutions were performed using an Agilent Cary 60 UV-Vis spectrophotometer at room temperature. The calibration curve of CEPA was constructed from various solutions obtained by dilution of a stock solution of pure CEPA in methanol.

DLS/zeta potential. Dynamic Light Scattering (DLS) and zeta potential measurements were performed using a Malvern Zetasizer Nano S instrument at 25 °C. All measurements were performed using a diluted dispersion at 0.03 wt% in Milli-Q water. The *Z*-average hydrodynamic diameter (D_Z) and polydispersity index (PDI) were calculated from 3 repeat measurements using the Stokes–Einstein equation, which assumes perfectly monodisperse, non-interacting spheres.

Transmission electron microscopy (TEM). Dry-state transmission electron microscopy (TEM) imaging was performed using an FEI TECNAI F20 microscope at an S3 acceleration voltage of 200 kV. All aqueous samples were diluted in Milli-Q water to 0.03–0.05 wt% and then deposited onto formvar/carbon film coated copper grids (400 mesh). After 90 s, the excess sample was blotted from the grid and the grid was stained with an aqueous 1 wt% uranyl acetate (UA) solution for 1 min prior to blotting, drying and microscopic analysis.

Results and discussion

In preliminary experiments, the synthesis of non-modified Boc-PεLL using the Ugi MCR of Boc-Lys (1.0 eq.) with *tert*-butyl isocyanide (1.3 eq.) and formaldehyde (1.3 eq.) in MeOH/water (1/1 v/v) was performed for 24 hours, 48 hours and 96 hours. The obtained results (Table S1†) show that higher molar masses can be obtained by extending the reaction duration. However, the molar mass of the obtained polymers remains limited (M_n < 5.0 kg mol^{-1}). This is probably due to the presence of a side-reaction that gives rise to a six-membered ring, which is unable to propagate during polymerisation, as mentioned in the literature.[30]

Inspired by our report on the chain-end functionalisation of polypeptoids,[32] the synthesis of a macro-RAFT agent was achieved in a single step by the addition of a CTA during the Ugi polymerisation of Boc-lysine (Boc-Lys) (Scheme 1). The CEPA/Boc-Lys molar ratio was fixed at 0.05 : 0.95 throughout the present work. The resulting Boc-PεLL-TTC was purified by precipitation in cold diethylether. The removal of the Boc-protecting group was performed afterward in a mixture of dichloromethane/trifluoroacetic acid (1 : 1 v/v). Table 1 summarises the macromolecular characteristics of two Boc-PεLL-TTCs and their corresponding PεLL-TTCs used in the present work. Molar mass distributions of these polymers are shown in Fig. 2. The molar mass of the resulting Boc-PεLL-TTC is in the same range as that of Boc-PεLL obtained without the addition of CEPA under similar reaction conditions (24 or 48 hours).

Fig. 1 shows the ^{1}H-NMR spectra of Boc-PεLL, Boc-PεLL-TTC and CEPA. The addition of CEPA to the Ugi MCR of Boc-Lys successfully resulted in Boc-PεLL-TTC as confirmed by the presence of the methyl peak *g* that originated from CEPA at around 1.9 ppm, which is absent from pure Boc-PεLL. Furthermore, the characteristic signals of Boc-PεLL are present

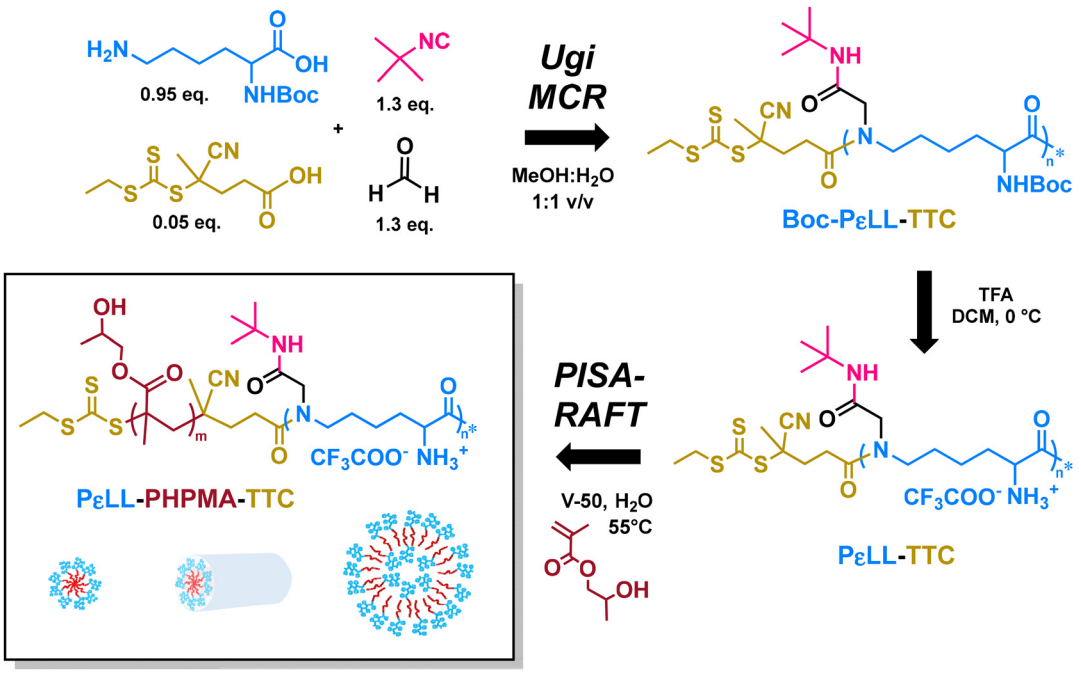

Scheme 1 General strategy for the synthesis of poly(ε-L-lysine) (PεLL)-decorated nanoparticles by sequential Ugi polymerisation and PISA-RAFT polymerisation in water.

Table 1 Macromolecular characteristics of Boc-PεLL-TTC (entries a) and their corresponding PεLL-TTC (entries b) obtained after Boc-deprotection

			SEC[b]		
Entry	macroCTA	$M_{n,\,UV}$[a] (g mol^{-1})	$M_{n,\,SEC}$ (g mol^{-1})	$M_{w,\,SEC}$ (g mol^{-1})	$Đ$
1a[c]	Boc-PεLL$_{1.5k}$-TTC	1800	2300	4200	1.82
1b	PεLL$_{1.5k}$-TTC	1500	6700	8900	1.36
2a[d]	Boc-PεLL$_{2.9k}$-TTC	2100	4500	6000	1.35
2b	PεLL$_{2.9k}$-TTC	2900	10 900	13 400	1.23

[a] Determined by UV-Vis absorption of TTC. [b] Eluent: DMF + 5 mM NH_4BF_4 at 50 °C, PEG calibration. [c] 24 hour reaction. [d] 48 hour reaction.

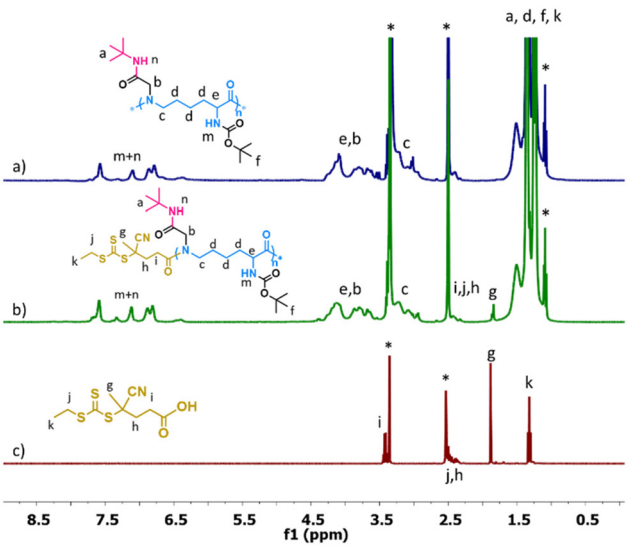

Fig. 1 ^{1}H-NMR spectrum of (a) Boc-PεLL, (b) Boc-PεLL-TTC, and (c) pure CEPA in DMSO-d_6 confirming the success in the synthesis of Boc-PεLL-TTC using the Ugi multicomponent reaction, * indicates the residual solvent.

with methylene protons of the PεLL and methyl protons of the *tert*-butyl groups located from 1.0 ppm to 1.6 ppm. Protons adjacent to amide functions are found between 2.8 ppm and 4.4 ppm whereas protons of amide functions are present between 6.2 ppm and 7.8 ppm. In addition, the ^{13}C-NMR spectrum of these three materials (ESI, Fig. S1†) also indicates a characteristic peak of methyl carbon at 12.8 ppm, which is observed in CEPA yet absent in Boc-PεLL. Unfortunately, other characteristic peaks of CEPA are not observable in the ^{1}H-NMR spectrum for they are obscured by overlapping signals from Boc-PεLL.

For further investigation, MALDI-ToF analysis was performed on two Boc-PεLL-TTC macroCTAs (ESI, Fig. S2†). The obtained results confirm the integrity of the polymer structure given by a series of peaks with $\Delta(m/z) \approx 341$ corresponding to a repeating unit of Ugi derivatives Boc-PεLL. More importantly, evidence for the presence of the trithiocarbonate function was also obtained from MALDI-ToF results (yellow triangle species, ESI, Fig. S2†). However, the signals from those species are less intense probably due to the sensibility of trithiocarbonate functions to MALDI measurement as reported elsewhere.[44]

To obtain water-soluble PεLL-TTC, the Boc protecting group was removed in a mixture of dichloromethane/trifluoroacetic acid (1 : 1 v/v) at 0 °C for 3–4 hours.

The disappearance of signals at 1.3 ppm in the ^{1}H-NMR spectra of polymers after deprotection and purification (ESI, Fig. S3†) indicates successful quantitative elimination of the Boc protecting group. In accordance, ^{19}F-NMR shows the presence of trifluoroacetate counterions (ESI, Fig. S4†). ^{13}C-NMR further confirms the disappearance of peaks that originated from the *tert*-butyl group after Boc deprotection (ESI, Fig. S5†).

Molar masses of PεLL-TTC were then characterised by chain-end analysis *via* UV-Vis absorption and size exclusion chromatography (SEC). The results of these analyses are summarised in Table 1. First, quantification of TTC by UV-Vis absorption at λ = 305 nm in methanol was performed based on a calibration curve of pure CEPA (Fig. S6, ESI†). $M_{n,UV}$ can be deduced from the concentration of TTC as given by eqn (1) (ESI†) assuming that each polymer chain bears one TTC. As expected, polymers obtained from the Ugi MCR over a 48 hour reaction have higher molar masses, 2100 g mol^{-1} for Boc-PεLL-TTC (entry 2a, Table 1) and 2900 g mol^{-1} for PεLL-TTC (entry 2b, Table 1) in comparison with 1800 g mol^{-1} (entry 1a, Table 1) and 1500 g mol^{-1} (entry 1b, Table 1), respectively, for those obtained over 24 hours. SEC in DMF (+5 mM NH_4BF_4 with PEG calibration) was also performed to obtain relative $M_{n,SEC}$ and dispersity of Boc-PεLL-TTC as well as PεLL-TTC, as shown in Fig. 2. The results obtained from SEC and UV-Vis confirm the difference in molar mass at varying Ugi MCR reaction times, *i.e.* the longer the reaction, the greater the chain length. However, $M_{n,\ UV}$ is smaller than $M_{n,\ SEC}$ for all studied polymers, which is expected because the calculation of $M_{n,\ UV}$ was performed by assuming 100% chain-end functionalisation. Furthermore, $M_{n,\ SEC}$ was obtained as relative M_n with PEG calibration in DMF. As the chain-end functionalisation of PεLL was carried out *in situ* during the polycondensation reaction, there are possibly non-functionalised Boc-PεLL molecules mixed with functionalised Boc-PεLL-TTC. The difference between $M_{n,\ UV}$ and $M_{n,\ SEC}$ is particularly significant for the cationic PεLL-TTC. This is because in SEC measurement, the charged nature of PεLL-TTC causes $M_{n,\ SEC}$ to shift to a higher molar mass. This shift can be attributed to the altered interaction of the polymers with the column material. Nevertheless, $M_{n,\ UV}$ before and after Boc-deprotection of the same polymer remains in the same range of molar mass, indicating that the TTC group remains intact after deprotection with trifluoroacetic acid. Due to the importance of quantifying TTC in the subsequent RAFT-PISA process, $M_{n,\ UV}$ was used as the reference value for further experiments. The macroCTAs are therefore denoted by their corresponding $M_{n,\ UV}$ values as PεLL$_{1.5k}$-TTC and PεLL$_{2.9k}$-TTC.

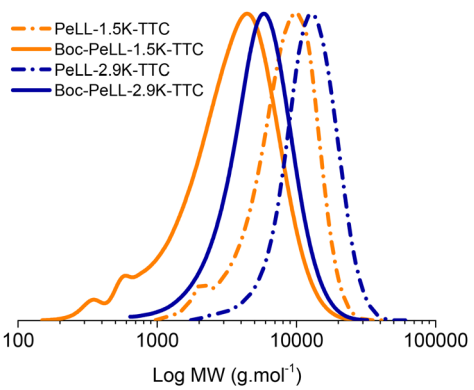

Fig. 2 Molar mass distribution of different Boc-PεLL-TTC and PεLL-TTC given in Table 1. SEC measurements were performed in DMF (+NH_4BF_4 5 mM) at 50 °C with PEG calibration.

The resulting hydrophilic PεLL-TTC compounds then served as macroCTAs in the aqueous RAFT polymerisation of HPMA at 55 °C (see Scheme 1). Table 2 summarises the results of chain extension of PεLL$_{1.5k}$-TTC with HPMA in water at 55 °C for 20 hours of reaction using V50 as an initiator. Under studied conditions, monomer conversion was >90% for all experiments with most achieving quantitative conversion. The molar mass after RAFT polymerisation of final formulations was analysed by SEC. These results are presented in Fig. S7, ESI.† Overall, except for DP$_0$ = 70, the increase in DP$_{0,\ PHPMA}$ gave rise to the molar mass of the obtained copolymers, featuring efficient chain extension. Though the inevitable presence of non-functionalised PεLL is noticed for all experiments, these signals are reduced in intensity when a higher DP is expected.

At the end of polymerisation, except for DP$_0$ = 70 at 15 wt%, final solutions were obtained as a stable dispersion given by their visual appearance (Fig. S8†). As is typical in the PISA process, nanoparticles are formed progressively as the polymerisation proceeds. Their formation causes light scattering, resulting in a transition to a turbid or milky-white appearance. Digital photos of polymer solutions, DLS results and TEM images of the final formulation can be found in ESI, Fig. S8–S10,† respectively. Fig. 3a illustrates the phase diagram of PεLL$_{1.5k}$-*b*-PHPMA as a function of monomer content and DP$_0$ with representative TEM images of different morphologies obtained during the PISA process. Overall, various morphologies were obtained from PεLL$_{1.5k}$-TTC by the PISA-RAFT process with HPMA at 5 wt%, 10 wt% or 15 wt% monomer content. First of all, at DP$_0$ = 10, based on the visual appearance of the final formulation, an evolution in morphology was expected with a turbid solution (5 wt%) giving spherical micelles, viscous solution at 10 wt% giving a mixture of spheres and short worm-like particles, and only gel at 15 wt% giving a fiber structure. Using TEM, a mixture of small spheres and short worm-like particles is observed from these three formulations. Unusual globular morphologies that appear intermediate or ill-defined may arise from the short HPMA chains used in these experiments, which may result in an unstable packing parameter, preventing the system from reaching well-defined equilibrium morphologies. Higher resolution TEM images of the short worm-like structures are presented in Fig. S10.† In agreement, DLS results show large polydispersity and significant deviation in particle size among number,

Table 2 Summary of PεLL$_{1.5k}$-TTC chain extension with HPMA by RAFT polymerisation in aqueous medium. Polymerisation conditions: [macroCTA]$_0$:[V-50]$_0$ = 1/0.2, T = 55 °C, t = 21 h, wt%: mass content of HPMA in water, DP$_0$ = [PεLL-TTC]$_0$/[HPMA]$_0$

						SEC$_{DMF,\ PEG\ calibration}$				DLS	
Entry	wt%	DP$_0$	Conv. (%)	DP$_{NMR}$	$M_{n,\ theo}$ [a] (g mol^{-1})	$M_{n,\ SEC}$ [a] (g mol^{-1})	$M_{w,\ SEC}$ (g mol^{-1})	$Đ$	TEM[b]	Z-Ave (d, nm)	PDI
P1	5	10	>99	10	2900	12 700	25 700	2.02	sS, sW	235	0.29
P2		20	>99	20	4380	18 800	65 800	3.49	S	310	0.02
P3		30	>99	30	5820	17 300	99 500	5.74	S	376	0.01
P4		50	91	46	8052	28 300	163 200	5.78	V	583	0.07
P5		70	97	68	11 278	27 000	115 300	4.28	V	468	0.02
P6	10	10	>99	10	2940	11 600	19 300	1.67	sS, sW	45	0.19
P7		20	>99	20	4380	19 400	69 700	3.59	S	881	0.22
P8		30	>99	30	5820	16 400	75 400	4.60	V	730	0.21
P9		50	>99	50	8700	22 700	151 800	6.69	V	666	0.07
P10		70	>99	70	11 580	27 700	140 900	5.08	V	769	0.26
P11	15	10	>99	10	2940	11 400	18 000	1.58	sS, sW	73	0.12
P12		20	>99	20	4380	18 400	49 200	2.67	V	1934	0.63
P13		30	>99	30	5820	18 000	99 500	5.57	V	1383	0.68
P14		50	>99	50	8700	29 100	160 300	5.52	V	1444	1.00
P15		70	98	69	11 378	31 500	131 700	4.18	—	—	—

[a] $M_{n,\ theo}$ was calculated from conversion determined by ^{1}H-NMR and from $M_{n,\ UV}$. [b] Expected morphology: sS = small sphere, S = sphere, sW = short worm-like particle, and V = vesicle.

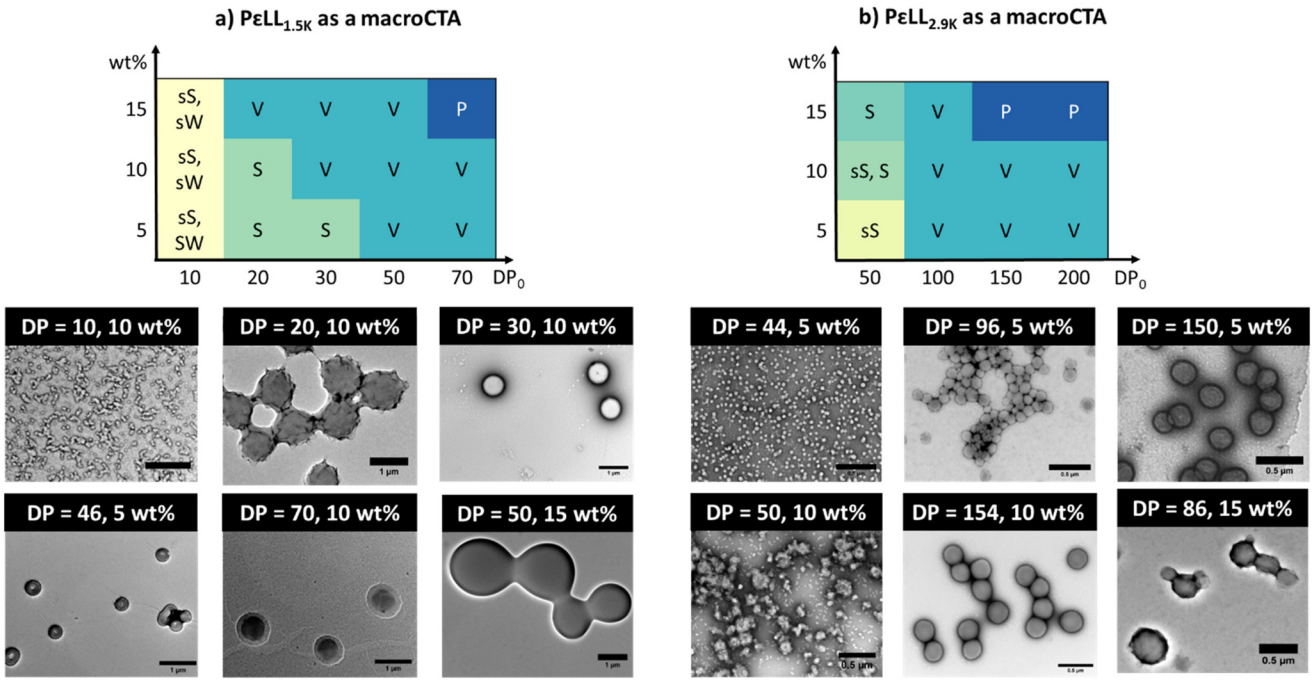

Fig. 3 Phase diagrams and representative TEM images of nanoparticles obtained by PISA-RAFT chain extension of (a) the PεLL$_{1.5k}$ macroCTA and (b) the PεLL$_{2.9k}$ macroCTA with HPMA in aqueous medium where DP$_0$ and the monomer content were varied. The scale bar is 1 μm for the PεLL$_{1.5k}$ macroCTA and 0.5 μm for the PεLL$_{2.9k}$ macroCTA. Abbreviation: sS = small sphere, sW = small worm-like particle, S = sphere, V = vesicle, and P = precipitation.

intensity and volume signals. The difference in the expected morphology and TEM image could be attributed again to the very short hydrophilic or HPMA block, which may cause instability upon dilution for TEM preparation, as reported in the literature for short poly(α-lysine) used as a macroCTA.[45] Specifically, as reported in the literature, nanostructures derived from short poly(α-lysine) (~780 g mol^{-1}) have been shown to lose stability upon dilution, leading to poorly defined structures observed in post-experiment TEM and DLS analyses. On the other hand, at a fixed monomer content of 5 wt%, as the proportion of DP$_{HPMA}$ increases, the morphology evolution of the diblock system was observed. In comparison with DP = 10, when the PHPMA block has DP = 20 or DP = 30, well-defined spherical structures were seen under TEM with

DLS giving a *Z*-average of 300–370 nm and PDI = 0.01–0.02; at a DP of ~50, a clear donut-type vesical structure was observed in TEM. At a higher monomer content, 10 wt% for example, the same phenomenon is observed with changes between DP_{PHPMA} = 10 and a higher DP_{PHPMA}. At DP = 70, a clear vesicular structure was seen in TEM images. Interestingly, when $DP_{PHPMA} \geq 20$, the change in the nanoparticle size appears to be mostly dependent on the monomer content rather than the DP of the PHPMA block. As expected, as the hydrophobic core gets bigger, the stability of the system is lost given by the formation of unstable aggregates and eventually precipitates are observed visually in the final solution.

To explore the effect of the PεLL chain length on the PISA process, another series of experiments was performed with $PεLL_{2.9k}$. A longer stabilising block is expected to form more stable nanoparticles with certain changes in particle sizes. Table S3 (ESI†) shows the results of chain extension of $PεLL_{2.9k}$-TTC with HPMA under aqueous conditions. Digital photos of the final appearances of these formulations are presented in Fig. S12 (ESI†). Fig. 3b shows the phase diagram and TEM images of acquired formulations. Overall, compared to $PεLL_{1.5k}$-TTC, the conversion of HPMA was lower, especially when a high DP_0 or high monomer concentration was targeted. In SEC profiles presented in Fig. S11,† molar masses achieved with the use of $PεLL_{2.9k}$-TTC also increased with an increase in target DP_{HPMA}. However, at 15 wt% and DP ≥ 150 (P26, P27, Table 3), precipitation was observed at 50–60% monomer conversion and SEC analysis was not performed as the polymer solution cannot be filtered over a 0.45 μm filter. Similar to $PεLL_{1.5k}$-TTC, the residual of non-functionalised PεLL was present in all formulations.

In terms of morphology, unlike $PεLL_{1.5k}$-PHPMA where some small worm-like particles can be found at a low DP, only spherical structures were found for the $PεLL_{2.9k}$-*b*-PHPMA system, which was also described in the literature for other ionic diblocks obtained by PISA-RAFT in aqueous medium.[46–48] As seen in Fig. 3b and Fig. S14,† at DP ~ 50, small spheres and a mixture of spheres with varying sizes were found at 5 wt% and 10 wt%. At a higher DP_{HPMA}, the particle sizes increase significantly. As expected, the size of the nanoparticles based on $PεLL_{2.9k}$-PHPMA is about twice as small as that obtained by $PεLL_{1.5k}$-PHPMA due to the longer stabilizer block.

To assess the stability of the nanoparticles, zeta-potential measurement was performed for formulations at 10 wt% monomer content. As seen in Fig. S15,† as expected, all nanoparticles show positive zeta potentials due to the cationic nature of PεLL as a stabilising block. Furthermore, the zeta potential of the obtained nanoparticles increases gradually with an increase of the PHPMA block length. When DP_{HPMA} < 140, all nanoparticles have zeta-potentials between 45 and 55 mV, indicating the good colloidal stability of ionic particles. However, at DP_{HPMA} = 154, the zeta potential of nanoparticles drops to ~22 mV, indicating the loss of ionic stability. This result is consistent with the visual observation where aggregation was found on the formulation of $PεLL_{2.9k}$-$PHPMA_{154}$.

SAXS analysis was performed for samples whose characteristic size observed in TEM was smaller than 50 nm including $PεLL_{1.5k}$-$PHPMA_{10}$ and $PεLL_{2.9k}$-$PHPMA_{50}$ prepared at 5 wt% and 10% monomer contents. For each of these samples, the scattering intensity as a function of wave vector is shown in Fig. S16, ESI.† The data were analysed in agreement with the TEM data and images using polydisperse hard spheres (eqn (2), ESI†). The fitting results are in good agreement with TEM and DLS analyses as given in Table S4, ESI.†

Finally, the kinetics of chain extension were studied on $PεLL_{2.9k}$ with a target degree of polymerisation DP_0 = 100 and 5 wt% solid content, to investigate the process kinetics during PISA-RAFT, as summarised in Fig. 4. As seen in Fig. 4a, under studied conditions, the chain extension of $PεLL_{2.9k}$-TTC with HPMA took place quite rapidly and reached >90% monomer conversion after ~70 minutes. An onset of polymerisation was observed at around 35 minutes, which is consistent with the visual observation where a rapid change in solution appear-

Table 3 Summary of $PεLL_{2.9k}$-TTC chain extension with HPMA by RAFT polymerisation in aqueous medium. Polymerisation conditions: $[macroCTA]_0:[V\text{-}50]_0$ = 1/0.2, *T* = 55 °C, *t* = 21 h, wt%: mass content of HPMA in water, $DP_0 = [PεLL\text{-}TTC]_0/[HPMA]_0$

						$SEC_{DMF,\ PEG\ calibration}$				DLS	
Entry	wt%	DP_0	Conv. (%)	DP_{NMR}	$M_{n,\ theo}$ [a] (g mol^{-1})	$M_{n,\ SEC}$ (g mol^{-1})	$M_{w,\ SEC}$ (g mol^{-1})	$Đ$	TEM[b]	*Z*-Ave (*d*, nm)	PDI
P16	5	50	>99	44	9240	18 800	42 500	2.26	sS	92	0.25
P17		100	87	96	16 740	31 500	124 700	4.00	sS, S	188	0.12
P18		150	>99	150	24 530	33 000	136 500	4.14	S	283	0.02
P19		200	>99	200	31 740	29 700	84 400	2.84	V	123	0.06
P20	10	50	>99	50	10 110	72 300	344 000	4.76	V	254	0.02
P21		100	80	80	14 430	57 100	187 000	3.28	V	396	0.03
P22		150	88	132	21 930	17 500	85 100	4.88	V	463	0.07
P23		200	77	154	25 100	84 700	417 200	4.93	V	319	0.04
P24	15	50	96	48	9820	21 700	53 400	2.46	V	374	0.20
P25		100	85	85	15 160	30 100	142 100	4.72	V	377	0.06
P26		150	57	86	15 300	NA	NA	NA	—	—	—
P27		200	51	102	17 610	NA	NA	NA	—	—	—

[a] $M_{n,\ theo}$ was calculated from conversion determined by ^{1}H-NMR and from $M_{n,\ UV}$. [b] Expected morphology, sS = small sphere, S = sphere, sW = short worm-like particle, and V = vesicle; NA: measurement was not performed due to impossibility of filtration.

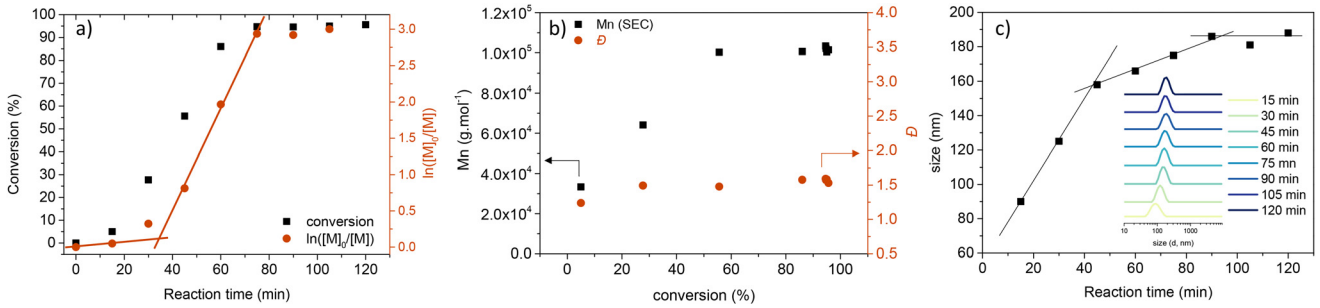

Fig. 4 Kinetics of chain extension of the PεLL$_{2.9k}$ macroCTA with HPMA (DP$_0$ = 100) at 5 wt% in terms of (a) conversion over the reaction time and pseudo-first linear plot, (b) molar mass and polydispersity evolution from SEC measurements with the exclusion of non-functionalised PεLL residuals, and (c) size evolution of the formed nanoparticles over time by DLS measurement.

ance from transparent to turbid was observed between 30 minutes and 45 minutes. Fig. S17a (ESI†) presents global molar mass evolution during the kinetics. It is seen that after 15 minutes (5% monomer conversion determined by ^{1}H-NMR), a second population appears on SEC profiles, which takes ~15% of the whole molar mass distribution. As the monomer conversion increases with the reaction time, a linear increase in molar mass was obtained until ~50% monomer conversion was given by the shift to a higher molar mass of the second population in the SEC profiles. Nonetheless, above 50% monomer conversion, no clear shift was observed. As discussed previously, as PεLL is positively charged, certain interactions with column materials could occur, leading to difficulty in molar mass separation.[47] Even though a bimodal molar mass distribution was observed due to the presence of non-functionalised PεLL, by excluding non-functionalised PεLL from the molar mass determination of the diblock, the molar mass distribution appears monomodal, and the weight fraction of this population (Fig. S17b, ESI†) increases with monomer conversion. The molar mass dispersity of the obtained diblock copolymers also remains around 1.5, featuring a relatively controlled polymerisation.

In terms of size evolution as presented in Fig. 4c, the diameter of the nanoparticles increases with the reaction time and monomer conversion. Three regimes can be observed in the evolution of the nanoparticle size. The first regime corresponds to the onset of polymerisation, with the initial formation of nanoparticles observed when monomer conversion is below 30%. Even at a slow monomer conversion of ~5% at 15 minutes, small particles of ~90 nm were already formed, which increased to ~125 nm at ~25% monomer conversion. After 35 minutes, as shown in Fig. 4a, micelle structures were formed and gradually increased in size due to an increase in monomer conversion. Once the monomer conversion reached >90%, almost no change in particle size was observed by DLS. TEM images taken for solution at 5%, 55.6% and 95.6% monomer conversion (Fig. S18, ESI†) also confirm the evolution in particle sizes obtained by DLS.

Lastly, the presence of non-functionalised PεLL is consistently observed throughout this work. This is inevitable, as during the Ugi MCR polymerisation, CEPA competes with the carboxylic acid group of Boc-Lys rather than being selectively incorporated. Technically, due to the similar molar masses of non-functionalised PεLL and PεLL-TTC, separating them using conventional purification methods such as dialysis, precipitation, or centrifugation poses a major challenge. Nonetheless, for the particle formation during the PISA process, these non-functionalised PεLL molecules appear to act as a co-stabiliser for the PεLL-PHPMA system with prospective ionic interaction between the charges, proven by a low to very low PDI (0.02–0.25) obtained by DLS measurements. Further study to synthesise PεLL-TTC with better chain-end fidelity may provide deeper insights into the role of non-functionalised PεLL in the self-assembly of PεLL-PHPMA during the PISA process, which is essential regarding the application of this system in biological fields.

Conclusions

In conclusion, this work provides a proof of concept for the successful one-pot synthesis of hydrophilic polypeptoids *via* the Ugi multicomponent reaction (MCR), using PεLL-TTC as a macroCTA for the PISA-RAFT process. The chain extension of PεLL-TTC with HPMA in aqueous medium proceeds as a controlled polymerisation, despite the presence of non-functionalised PεLL in the formulation, which shows minimal interference with the formation of PεLL-HPMA nanoparticles of various morphologies (small spheres, small worm-like particles and small vesicles). Furthermore, the size of these nanoparticles was demonstrated to depend on target DP$_{HPMA,\ 0}$ and the monomer content as demonstrated by DLS results. In addition, zeta potential measurements showed good stability of the formed particles and confirmed the ionic colloidal stabilisation nature of PεLL featuring zeta-potential values between 45 and 55 mV.

Given the combinatorial versatility of the Ugi MCR to prepare polypeptoids, with the robustness of PISA-RAFT in producing nanoparticles with diverse morphologies and tuneable sizes, this novel combination of the Ugi MCR and PISA is expected to advance the synthesis and self-assembly of novel functional macromolecules.

Author contributions

The manuscript was written through contributions of all authors. All authors have given approval to the final version of the manuscript.

Data availability

All raw data generated and analyzed during the course of this study are securely stored at the Institut de Chimie et des Matériaux Paris-Est (ICMPE), CNRS. These include all experimental procedures, nuclear magnetic resonance (NMR) spectroscopy data, dynamic light scattering (DLS) measurements, transmission electron microscopy (TEM) images, size exclusion chromatography (SEC) data, and other relevant characterization files supporting the results and conclusions presented in the manuscript.

These datasets are not publicly accessible. However, they are available from the corresponding author upon request.

Conflicts of interest

There are no conflicts to declare.

Acknowledgements

This work was supported by financial funding from CNRS INC Emergence. We also acknowledge the support from the CAP and MIC ICMPE platforms, DIM MaTerRe, and the Île-de-France region. A.D. thanks the F.R.S.-FNRS for financial support.

References

1 J. Wan, B. Fan and S. H. Thang, *Chem. Sci.*, 2022, **13**, 4192–4224.
2 H. Phan, V. Taresco, J. Penelle and B. Couturaud, *Biomater. Sci.*, 2021, **9**, 38–50.
3 C. Liu, C.-Y. Hong and C.-Y. Pan, *Polym. Chem.*, 2020, **11**, 3673–3689.
4 C. Grazon, P. Salas-Ambrosio, E. Ibarboure, A. Buol, E. Garanger, M. W. Grinstaff, S. Lecommandoux and C. Bonduelle, *Angew. Chem., Int. Ed.*, 2020, **59**, 622.
5 D. B. Wright, M. A. Touve, L. Adamiak and N. C. Gianneschi, *ACS Macro Lett.*, 2017, **6**, 925–929.
6 S. Varlas, J. C. Foster and R. K. O'Reilly, *Chem. Commun.*, 2019, **55**, 9066–9071.
7 M. J. Derry, L. A. Fielding and S. P. Armes, *Prog. Polym. Sci.*, 2016, **52**, 1–18.
8 L. Lei, N. Patil, A. Arnoux, C. Le Cœur, Y. de Rancourt de Mimérand, D. Grande, B. Le Droumaguet, X. Feng, Y. Gnanou and B. Couturaud, *Macromolecules*, 2024, **57**, 10513–10521.
9 H. Phan, R. Cavanagh, D. Destouches, F. Vacherot, B. Brissault, V. Taresco, J. Penelle and B. Couturaud, *ACS Appl. Polym. Mater.*, 2022, **4**, 7778–7789.
10 H. Phan, R. Cavanagh, P. Jacob, D. Destouches, F. Vacherot, B. Brugnoli, S. Howdle, V. Taresco and B. Couturaud, *Polymers*, 2023, **15**, 3070.
11 N. Audureau, F. Coumes, J.-M. Guigner, T. P. T. Nguyen, C. Ménager, F. Stoffelbach and J. Rieger, *Polym. Chem.*, 2020, **11**, 5998–6008.
12 D. Ikkene, J.-L. Six and K. Ferji, *Eur. Polym. J.*, 2023, **188**, 111848.
13 J. Sun and R. N. Zuckermann, *ACS Nano*, 2013, **7**, 4715–4732.
14 N. Gangloff, J. Ulbricht, T. Lorson, H. Schlaad and R. Luxenhofer, *Chem. Rev.*, 2016, **116**, 1753–1802.
15 K. Klinker and M. Barz, *Macromol. Rapid Commun.*, 2015, **36**, 1943–1957.
16 A. M. Clapperton, J. Babi and H. Tran, *ACS Polym. Au*, 2022, **2**, 417–429.
17 D. Zhang, S. H. Lahasky, L. Guo, C.-U. Lee and M. Lavan, *Macromolecules*, 2012, **45**, 5833–5841.
18 M. Hartweg, C. J. C. Edwards-Gayle, E. Radvar, D. Collis, M. Reza, M. Kaupp, J. Steinkoenig, J. Ruokolainen, R. Rambo, C. Barner-Kowollik, I. W. Hamley, H. S. Azevedo and C. R. Becer, *Polym. Chem.*, 2018, **9**, 482–489.
19 A. Ma, X. Yu, M. Liao, W. Liu, S. Xuan and Z. Zhang, *Macromol. Rapid Commun.*, 2023, **44**, 2200301.
20 R. Kakuchi, *Angew. Chem., Int. Ed.*, 2014, **53**, 46–48.
21 B. Couturaud, Z. H. Houston, G. J. Cowin, I. Prokeš, J. C. Foster, K. J. Thurecht and R. K. O'Reilly, *ACS Macro Lett.*, 2019, **8**, 1479–1483.
22 A. K. Pearce, A. Travanut, B. Couturaud, V. Taresco, S. M. Howdle, M. R. Alexander and C. Alexander, *ACS Macro Lett.*, 2017, **6**, 781–785.
23 E. Ruijter and R. V. A. Orru, *Drug Discovery Today: Technol.*, 2013, **10**, e15–e20.
24 E. Ruijter, R. Scheffelaar and R. V. A. Orru, *Angew. Chem., Int. Ed.*, 2011, **50**, 6234–6246.
25 O. Kreye, O. Türünç, A. Sehlinger, J. Rackwitz and M. A. R. Meier, *Chem. – Eur. J.*, 2012, **18**, 5767–5776.
26 A. C. Boukis, A. Llevot and M. A. R. Meier, *Macromol. Rapid Commun.*, 2016, **37**, 643–649.
27 A. C. Boukis and M. A. R. Meier, *Eur. Polym. J.*, 2018, **104**, 32–38.
28 W. Konrad, F. R. Bloesser, K. S. Wetzel, A. C. Boukis, M. A. R. Meier and C. Barner-Kowollik, *Chem. – Eur. J.*, 2018, **24**, 3413–3419.
29 P.-K. Dannecker, A. Sehlinger and M. A. R. Meier, *Macromol. Rapid Commun.*, 2019, **40**, 1800748.
30 X. Zhang, S. Wang, J. Liu, Z. Xie, S. Luan, C. Xiao, Y. Tao and X. Wang, *ACS Macro Lett.*, 2016, **5**, 1049–1054.
31 P. Stiernet, B. Couturaud, V. Bertrand, G. Eppe, J. De Winter and A. Debuigne, *Polym. Chem.*, 2021, **12**, 2141–2151.
32 A. A. Samad, J. D. Winter, P. Gerbaux, C. Jérôme and A. Debuigne, *Chem. Commun.*, 2017, **53**, 12240–12243.

33 Y. Tao, S. Wang, X. Zhang, Z. Wang, Y. Tao and X. Wang, *Biomacromolecules*, 2018, **19**, 936–942.
34 M. Saimura, M. Takehara, S. Mizukami, K. Kataoka and H. Hirohara, *Biotechnol. Lett.*, 2008, **30**, 377–385.
35 I.-L. Shih, M.-H. Shen and Y.-T. Van, *Bioresour. Technol.*, 2006, **97**, 1148–1159.
36 J.-N. Liu, S.-L. Chang, P.-W. Xu, M.-H. Tan, B. Zhao, X.-D. Wang and Q.-S. Zhao, *J. Agric. Food Chem.*, 2020, **68**, 1101–1109.
37 Y. Wang, L. Wang, Y. Hu, J. Qin and B. Yu, *Int. J. Biol. Macromol.*, 2024, **262**, 129513.
38 A. Traeger and M. N. Leiske, *Biomacromolecules*, 2025, **26**, 5–32.
39 M. Li and Y. Tao, *Polym. Chem.*, 2021, **12**, 1415–1424.
40 B. Yang, Y. Zhao, X. Ren, X. Zhang, C. Fu, Y. Zhang, Y. Wei and L. Tao, *Polym. Chem.*, 2014, **6**, 509–513.
41 H. Wu, B. Yang, Y. Zhao, Y. Wei, Z. Wang, X. Wang and L. Tao, *Polym. Chem.*, 2016, **7**, 4867–4872.
42 B. Yang, Y. Zhao, C. Fu, C. Zhu, Y. Zhang, S. Wang, Y. Wei and L. Tao, *Polym. Chem.*, 2014, **5**, 2704–2708.
43 X. Pan, F. Zhang, B. Choi, Y. Luo, X. Guo, A. Feng and S. H. Thang, *Eur. Polym. J.*, 2019, **115**, 166–172.
44 A. Kerr, G. Moriceau, M. A. Przybyla, T. Smith and S. Perrier, *Macromolecules*, 2021, **54**, 6649–6661.
45 L. Luppi, T. Babut, E. Petit, M. Rolland, D. Quemener, L. Soussan, M. A. Moradi and M. Semsarilar, *Polym. Chem.*, 2019, **10**, 336–344.
46 M. Semsarilar, V. Ladmiral, A. Blanazs and S. P. Armes, *Langmuir*, 2013, **29**, 7416–7424.
47 V. Baddam, L. Välinen, L. Kuckling and H. Tenhu, *Polym. Chem.*, 2022, **13**, 3790–3799.
48 G. N. Smith, L. L. E. Mears, S. E. Rogers and S. P. Armes, *Chem. Sci.*, 2018, **9**, 922–934.